



Fragor61T: Parametric Loudspeaker

Diego Cardona, Santiago Vega

► To cite this version:

Diego Cardona, Santiago Vega. Fragor61T: Parametric Loudspeaker. Le mans Université. 2021.
hal-03935414

HAL Id: hal-03935414

<https://hal.science/hal-03935414v1>

Submitted on 6 Feb 2023

HAL is a multi-disciplinary open access archive for the deposit and dissemination of scientific research documents, whether they are published or not. The documents may come from teaching and research institutions in France or abroad, or from public or private research centers.

L'archive ouverte pluridisciplinaire **HAL**, est destinée au dépôt et à la diffusion de documents scientifiques de niveau recherche, publiés ou non, émanant des établissements d'enseignement et de recherche français ou étrangers, des laboratoires publics ou privés.



Fragor61T: Parametric Loudspeaker

Authors:

CARDONA Diego
VEGA Santiago

Advisors:

NOVAK Antonin
MELON Manuel

IMDEA M1 Project
Academic year 2021-2022

Contents

1	Introduction	4
2	Theoretical background	4
3	State of the Art	5
4	AM Modulation Techniques	5
4.1	Square-Root Amplitude Modulation	5
4.2	Double-Sideband Amplitude Modulation	6
5	Transducer characterization	7
5.1	Mechanical model	7
5.2	Electrical model	8
5.3	Acoustic model	9
6	Transducer Array	10
6.1	Array Design	11
6.2	Mechanical and electrical model	11
6.3	Acoustic model	12
6.4	Experimental results for the hexagonal array	14
6.4.1	Carrier signal frequency selection	15
6.4.2	Pressure level with respect to distance	15
6.4.3	Directivity patterns	16
6.5	Experimental results for the curved array	17
6.5.1	Pressure level with respect to distance	17
6.5.2	Directivity patterns	18
7	Additional system components	19
7.1	Audio input	19
7.2	DSP	19
7.3	Pre-amplifier	20
7.4	Power amplifier	21
7.5	Motors and WIFI Control	22
8	Conclusions	22
9	Future work	23

Appendix A Measurement conditions	24
Appendix B Amplifier Gain	24
Appendix C Pressure distribution for the curved array	25

1 Introduction

A parametric loudspeaker is a device that is able to reproduce a highly directive sound beam instead of the "classical" omnidirectional behaviour that most speakers possess. It works by exploiting the non-linearities of the propagation medium to demodulate an amplitude modulated ultrasonic signal into an audible sound. In addition to that, due to its narrow, focused beam, it can be easily reflected on objects to simulate a virtual source on its surface.

So, the purpose of this work is to construct, model and evaluate the behaviour of such a system. The focus lies in discerning the impact of the non-linearities of the system and juxtaposing them to its corresponding linear model and literature. Moreover, other topics of interest are the investigation, experimentation and implementation of different techniques to modify and improve the response of the loudspeaker. Such aspects include the amplitude modulation, array shape and user experience in general (incorporating wireless volume and position control and allowing the user to connect to the system by a common auxiliary cord).

Moreover, since this technology is relatively new and lends itself for versatility, many different application fields have not been delved into or can be improved. This project also lays ground for further investigation on the topic and proposes possible future research subjects.

2 Theoretical background

The propagation of sound in fluids consists in a non-linear process; that is especially true for high-level sound pressure signals. The cause is mainly due to heterogeneity of the density and compressibility along the medium caused by temperature, humidity and its general atomic composition; this leads to scattering and distortion [2] [22] [19].

Parametric loudspeakers seek to take advantage of this phenomenon in the air to create a highly directive, far-reaching sound beam that does not require a demodulation system, as this process is completed by the non-linearities of the air itself. Such devices are composed by linear arrays of closely-placed ultrasonic transducers to increase radiation efficiency, emitting the same exact high-frequency, amplitude modulated (AM) signal (where the carrier signal is in the ultrasonic range; and message, in the audible one) [14] [13] [11]. To achieve this, one can employ diverse methods; such investigations have been carried out for their application in acoustic spotlights in several works like [14] [7] [8] [6] [11]. Their evaluation ranges from studies about the distortion, power consumption and some even the implementation issues, audible bandwidth restrictions and array shapes [20].

The reason as to why an audible sound appears is that an end-fire array of virtual acoustic sources is created with the aforementioned configuration of transducers [18]. This is directly related to the Inter-Modulation Distortion (IMD) between the coincident carrier and message waves, i.e. two additional waves will surge from the non-linear interaction with frequencies $f_1 \pm f_2$, where f_1 and f_2 correspond to the frequencies of the carrier and message signals of the AM modulation. Plus, since one of those frequencies corresponds to an ultrasonic signal, the one created by the sum of the frequencies will not be perceivable. However, the one resulting from the difference will propagate and, when choosing f_1 and f_2 properly, it can become audible, as only the phases of the plane waves will be added [2] [22] [21] [19]. This theory was the basis of a lot of works that were mostly focused on underwater applications, restricting the applications to the near-field, where "the ultrasonic source exhibits strong self-interference effects from interfering emissions from different locations on the source" [14].

However, this is not very useful for fluids like air, as the absorption coefficient of water at high frequencies is greater than that in the air. So, due to this, the audible sound in air will only be present in the far-field, where the field is more uniform and the distance from the source is greater than the Rayleigh

distance [2] [9] [5]. Nevertheless, this can be extended to an advantage when considering that the sound will take longer to dissipate as well. Thus, the sound beam will propagate several meters more than most of its "normal" audible wavelength counterparts [14].

Moreover, it is known that the sound directivity is directly related to the ratio between the wavelength and the geometric dimensions of the source, i.e. the smaller the source and the lower the frequency, the more omnidirectional it behaves. So, normally, to get a very narrow beam, the size of the source is increased, as higher frequencies result in inaudible sounds. Nonetheless, parametric loudspeakers transmit only ultrasound, whose wavelengths are just millimeters in length; meaning that they are much smaller than the source and produce "a highly directional beam of audible sound results" [14] [13]. Then, some of the intrinsic properties of ultrasound will be extended to the audible signal after demodulation.

Furthermore, regarding the modelling of this phenomenon, it is not uncommon to approximate some of these non-linear effects as linear or quasilinear ones, like different approaches to solving the Khokhlov-Zabolotskaya-Kuznetsov (KZK) and Burgers's equation. This has been done in numerous works and shown promising results; like Berkay in [2], Pompei in [14] and Westerveld in [21]. Nevertheless, the linear approximation may not be sufficient, as the directivity gets more omnidirectional as the frequency lowers, but this may not be true in real-life transducers. This, due to the intrinsic non-linearities of the device like mechanical and electrical characteristics, for example [14].

3 State of the Art

Even though the technology for parametric arrays has been present since the late 50s for underwater applications [4]; and that same approach was implemented for its airborne equivalent around the 80s [22], it is not until the early 2000s [13] [14] that the feasibility of a parametric loudspeaker is palpable. Then, improvements on the control scheme of the techniques needed for the transducer to function properly were presented, as well as amelioration in the sound quality in general.

Since then, the implementation of this technology has slowly gained momentum; with Holosonics being its pioneer. Some of the applications range from implementation on Disney's Epcot, its use on different tradeshows, museums and even some hospitals [15]. In addition to that, there are other corporations focusing on commercializing these devices, like Soundlazer, Focusonics, Panphonics, Hypersound, etc.

Furthermore, there has also been an increase of interest in the research community, investigating the impact of different geometrical, electrical, mechanical and acoustical aspects of the parametric array. Nevertheless, the main interest appears to be to solve the power and distortion problems that presents such a technology [6] [14] [7] [16].

4 AM Modulation Techniques

Since this technology is heavily tied to an elevated power consumption and the use of AM Modulation to encode the audible signal is a key aspect to achieve high pressure levels for the audible sound, the efficiency of this process is relevant. For this project, two main techniques are considered: Square-Root (SRAM) and Double-Sideband (DSB-AM).

4.1 Square-Root Amplitude Modulation

This method is based on Berkay's model, but has been improved since then [6]. It consists in applying the following envelope function $E(t)$ to the carrier signal:

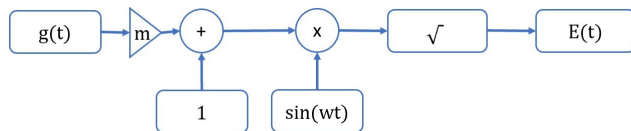


Figure 1: Square-Root Amplitude Modulation block diagram

where $g(t)$ is the message to be encoded and m is the modulation index.

Using such a method for a 40kHz signal yields a frequency response function (FRF) like the one presented in Fig. 3 (left). A more in-depth discussion on the choice of the carrier frequency is presented in Section 6.4.1. Nevertheless, a much larger bandwidth is needed for the emitter in comparison to other alternatives, as the square-root operation introduces infinite harmonics [6].

4.2 Double-Sideband Amplitude Modulation

In a similar manner, another alternative is to remove the square-root operation to avoid the harmonics generated by it. So, the envelope becomes just

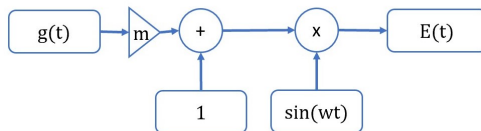


Figure 2: Double sided band modulation block diagram

This expression results in what is presented in Fig. 3 (right) for the same 40kHz signal. As expected, the bandwidth is significantly reduced. Although literature indicates that this method presents a higher Total Harmonic Distortion (THD) for a high value for m than the previous method indicated, to achieve a high pressure level for the audible signal, this requirement also needs to be fulfilled.

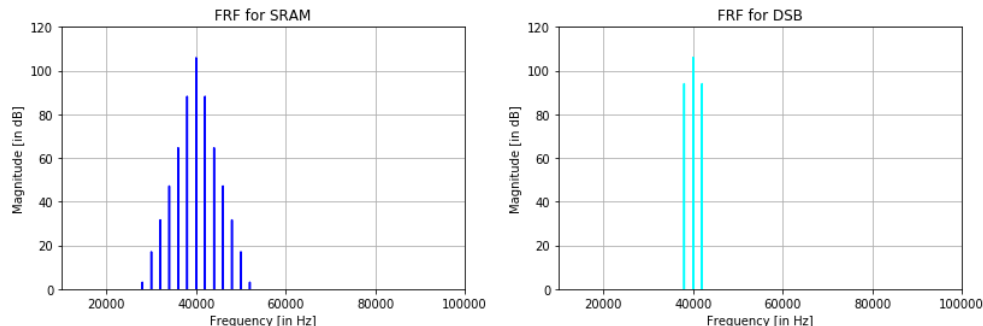


Figure 3: FRF for a 40kHz signal using different amplitude modulation techniques: SRAM (left) and DSB-AM (right).

So, because the transducer's bandwidth is not as wide as that shown in Fig. 3 (see Figs. 5 and 6), which would lead to distortion, and due to the fact that the function generators at the disposal use DSB-AM, all tests completed for this work are done using this technique. Albeit using digital signal processing allows to alter this method, the availability was limited at the time the tests were completed.

5 Transducer characterization

To properly predict, model and simulate the behaviour of the array, a modelization of a single transducer is needed first. For this, the 400ST120 ultrasonic transducer is used for all the measurements and as reference for the simulated results, as this is the one used for the parametric loudspeaker.

5.1 Mechanical model

Mechanically, each ultrasonic loudspeaker may be approximated as a single degree of freedom (SDOF) system like the one in Fig. 4. So, first, the Frequency Response Functions (FRFs) for each transducer is measured to get a sense of the position of the resonance, as well as their magnitude and phase. The latter is mostly due to the fact that not all brands provide reliable information about the polarity of the devices, which may have a significant impact on the resulting array [3]. The experimental results are shown in Fig. 5.

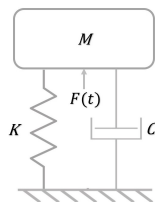


Figure 4: Single degree of freedom system mechanical model.

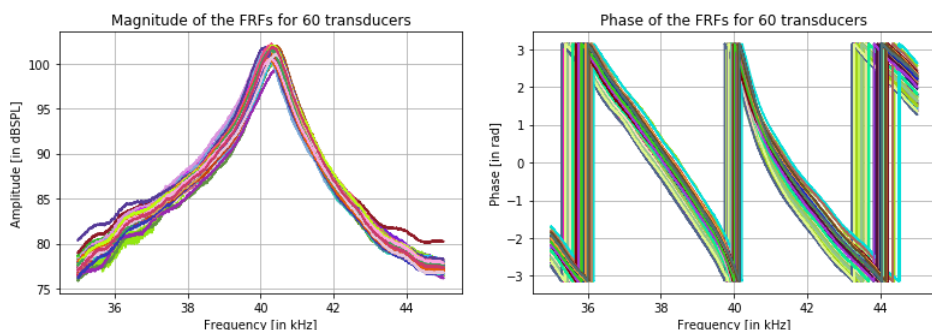


Figure 5: Magnitude and phase of the FRF of each individual ultrasonic loudspeaker.

Since the overall behaviours of all transducers are very similar (and the phases are not inverted for any of them), it is convenient to average the behaviour and to create a simulated version that fits this comportment. For this, a parameter variation for each of the coefficients for the SDOF system is carried out to get an approximation of the mechanical behaviour of the transducers; both results are juxtaposed in Fig. 6.

This model shows great accuracy near the resonance peak (which is located at 40.29kHz with an amplitude of 100.97dB SPL) and for lower frequencies. Even if the approximation is not very accurate for higher frequencies, it is not very far off and the operation point will still be chosen to be at the resonance. The values for the SDOF parameters are the following: $M = 10^{-3}\text{kg}$, $K = 64116503\text{N/m}$ and $C = 5.7\text{kg/s}$, where M is the mass, K the stiffness and C the damping coefficient. In addition to that, it is possible to calculate the mechanical quality factor; it results in $Q_m = 44.4$.

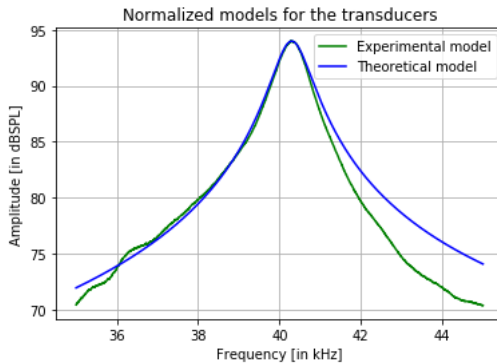


Figure 6: Comparison of the averaged experimental FRFs of the ultrasonic loudspeakers and the theoretical model proposed.

5.2 Electrical model

Moreover, one can also take into account the electrical model of the transducers. For the measurements, the circuit in Fig. 7 is used. These consist in doing multiple mensurations utilizing an LCR meter at different frequencies and taking note of their impedance, Z , and angle. This way, it is more convenient to discern the capacitive, C , and inductive L , components at the different frequency bands and decide for a model by employing the general equation for the electrical impedance

$$Z = R + j \left(\frac{1}{\omega C} + \omega L \right) \quad (1)$$

where ω is the angular frequency and R the electrical resistance.

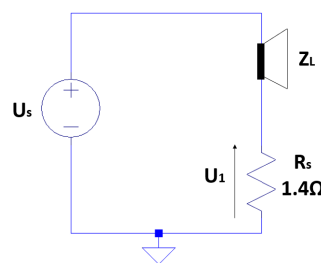


Figure 7: Circuit used for the measurements of the electrical components of the transducers.

So, the impedance for a single transducer is illustrated in Fig. 8. Here, one can observe how the impedance decreases with frequency; also, one can note a slight increase at the mechanical resonance peak as well. In addition to that, it is clear that, for the most part, the reactance behaves like a purely capacitive one, as the phase remains negative for all frequencies (except at the resonance). Furthermore, due to the overall shape of the impedance curve, it is possible to deduce that the resistor and capacitor used to model the electrical comportment are connected in series.

Thus, one can deconstruct the previous graph into its resistive and capacitive components, as depicted in Fig. 9, to have a sense of the values of the electrical parameters of the transducer.

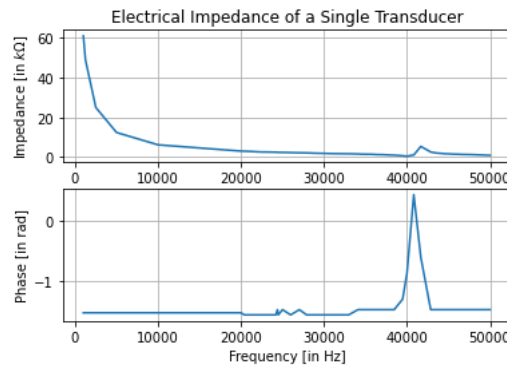


Figure 8: Electrical Impedance of a single transducer

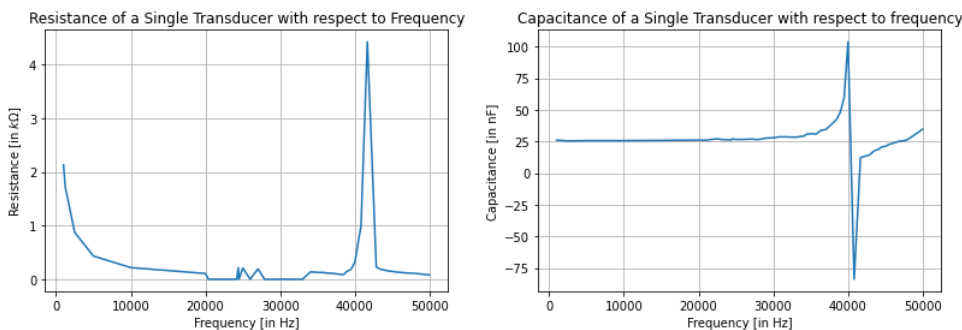


Figure 9: Resistive (left) and capacitive (right) behaviours of a single transducer.

5.3 Acoustic model

Finally, to get a representation of the corresponding particle velocity, v , and pressure, p , one can model the system as a baffled circular piston of radius a . Thus, the in-axis pressure at a distance r from the origin is

$$p(r, \omega) = \frac{j\omega\rho_0|v|S}{2\pi r} \frac{2J_1(k \operatorname{asin}(\theta))}{\operatorname{asin}(\theta)} e^{-j\frac{\omega}{c}r} \quad (2)$$

where k is the angular wavenumber of the signal transmitted; $|v|$ is the RMS value of the particle velocity; S , the surface area of the piston; J_1 , the Bessel function of the first order and kind; θ , the incidence angle to the listening point; and c , the celerity in air.

However, one must also take other factors into account, like the fact that the amplitude of the pressure depends on the input RMS voltage provided to the transducer, U_{rms} , and the ponderation of the amplitude according to θ , i.e. the gain G . This will then result in the following

$$p(r, \omega) = U_{rms} \frac{j\omega\rho_0|v|SG}{2\pi r} \frac{2J_1(k \operatorname{asin}(\theta))}{\operatorname{asin}(\theta)} e^{-j\frac{\omega}{c}r} \quad (3)$$

Albeit, the value for $|v|$ is still unknown. So, one can solve for it from Eq. 3 using the RMS value of the measured pressure at the resonance point in Fig. 5. Also, as the measurement is carried out for $\theta = 0$, leading to unitary gain, the expression for the velocity is then

$$|v| = \frac{r|p|}{U_{rms}f\rho S} \quad (4)$$

where f is the frequency of the signal and ρ is the air density. This leads to the behaviour for the average particle velocity shown in Fig. 10, where it is possible to extract the fact that $|v| = 0.12 \frac{m}{s}$ at the resonance peak ($f = 40.29 kHz$).

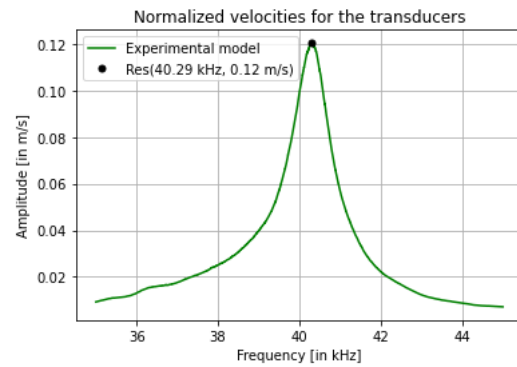


Figure 10: Average particle velocity for the ultrasonic transducers

Nevertheless, the values for the gain are still needed for different values of θ . These will be obtained by measuring the directivity pattern of the transducer. This experiment consists in taking numerous mensurations of the FRF for the different positions along the same plane. In this case, it is assumed that the response in the azimuth and elevation planes are the same, so only one of them is considered for the experiment. This leads to the behaviour shown in Fig. 11 for a 10° resolution at a $5cm$ - distance along the azimuth plane at $40kHz$ (which is close to the resonance frequency).

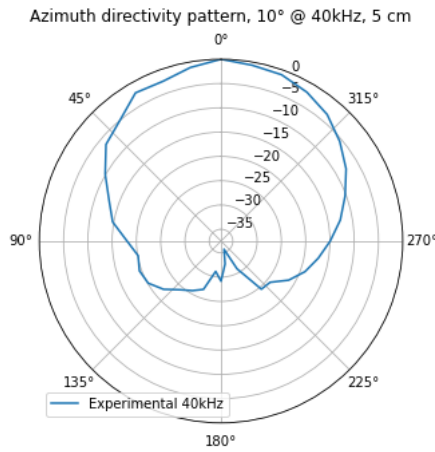


Figure 11: Experimental directivity pattern of a single transducer with a 10° resolution at a $5cm$ distance along the azimuth plane at $40kHz$.

6 Transducer Array

So, after having a general model for each of the ultrasonic transducers that will be employed for the parametric loudspeaker, it is possible to proceed to the analysis and theoretical representation of the array.

6.1 Array Design

The design of the array configuration is based on the fact that the transducers should be placed as close as possible to each other to maximize the radiation efficiency by occupying as much effective area inside the array as possible. Besides, the number of transducers is also a restriction, as one had only access to 61 of them. In addition to that, a curved alternative with its focal point at 30cm from the origin is also considered to verify if it improves the controllability of the resulting pressure beam, as presented in [12] and [17].

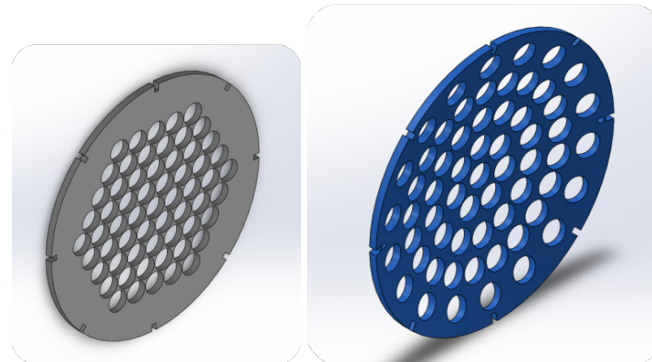


Figure 12: Hexagonal (left) and curved (right) array models

Thus, the designs shown in Fig. 12 surge; denoted from now on hexagonal and curved arrays; it is important to state that "the origin" for all measurements is located at the center of the middle transducer in both cases.

6.2 Mechanical and electrical model

Moreover, when considering the theoretical model of the array, it is evident to note that the transducers are mechanically independent of each other, so their overall behaviour (more importantly, the corresponding resonance frequency) of each individual component will remain unchanged no matter the shape of the array. Similarly, the electrical behaviour of the loudspeaker is independent of the placement of the components. However, in this case, the electrical impedance is modified with respect to the single transducer case, as they are connected in parallel. This leads to what is shown in Figs. 13 and 14.

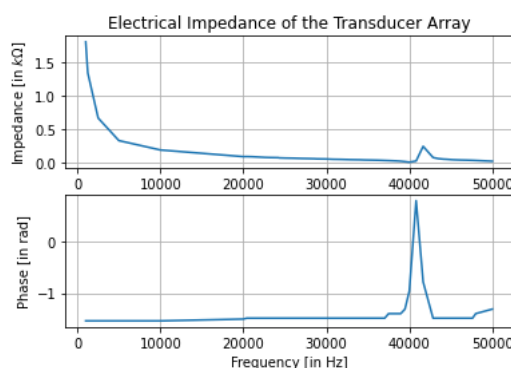


Figure 13: Electrical impedance of the transducer array.

As expected, the resistance is greatly reduced; and the capacitance, increased. However, the exact values are not what is expected, as a factor of 61 should correspond to connecting that amount

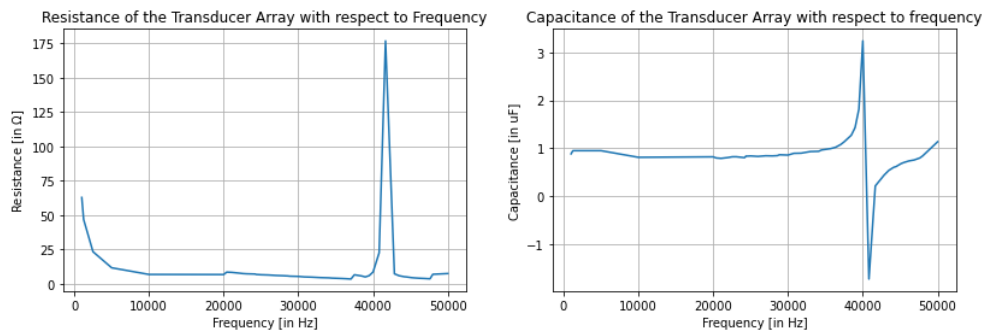


Figure 14: Resistance and capacitance of the transducer array with respect to frequency.

of transducers in parallel. This calls for a revision of the data, but, due to time constraints and some restriction access to the equipment, it was not possible to carry out.

6.3 Acoustic model

On the other hand, an impact of the transducer placing is expected for the acoustical characterization of the array. It is important to keep in mind that the presented model does not consider the impact of the non-linearities of the air and that are done for a 40kHz signal, as it matches the resonance frequency of the transducers.

Thus, to create this model, one must extrapolate the experimental directivity pattern values in Fig. 11 to those in the transducer array, i.e. assign a gain to the angles between each of the transducers in the array to the listening point (LP) with respect to the ones measured. Then, it is possible to employ Eq. 3 for each element of the two array configurations for both, the azimuth and elevation, planes and calculate the total pressure at the point of interest.

A couple results for the hexagonal array are shown in Fig. 15. It presents the pressure distribution along the hexagonal array at $LP(0 | 0 | 30\text{cm})$ (on the uppermost row of the graph) and at a 10° difference on each plane ($LP(5.209\text{cm} | 0 | 29.54\text{cm})$ on the azimuth one, on the left of the figure, and at $LP(0 | 5.209\text{cm} | 29.54\text{cm})$ for elevation; on the right). Their corresponding pressure levels are shown in Tab. 1.

Listening Point	Pressure Level
$LP(0 0 30\text{cm})$	126.0 dB SPL
$LP(5.209\text{cm} 0 29.54\text{cm})$	112.8 dB SPL
$LP(0 5.209\text{cm} 29.54\text{cm})$	116.2 dB SPL

Table 1: Pressure levels at the different LP for the hexagonal array for a 40kHz signal.

With these results, it is important to remark some facts. First, it is possible to note that the response between the azimuth and elevation planes are very similar (around 3dB SPL). Secondly, and more relevant for this particular application, there is a palpable drop in the overall pressure when displacing the listening point by only 10° . In any case, one can consider rotating the LP along each axis by maintaining the same radius to get the directivity patterns; they are illustrated in Fig. 16.

Here, it is possible to note that the system is very directive, because the magnitude along the polar plane as one moves away from the 0° decreases greatly (after a 10° difference they all have gains lower than -10dB). Also, the overall shape of the main lobe of the directivity patterns of both planes (which, in comparison to the rest, is the only relevant one) is very similar, reiterating the fact that they can be interchangeable if needed.

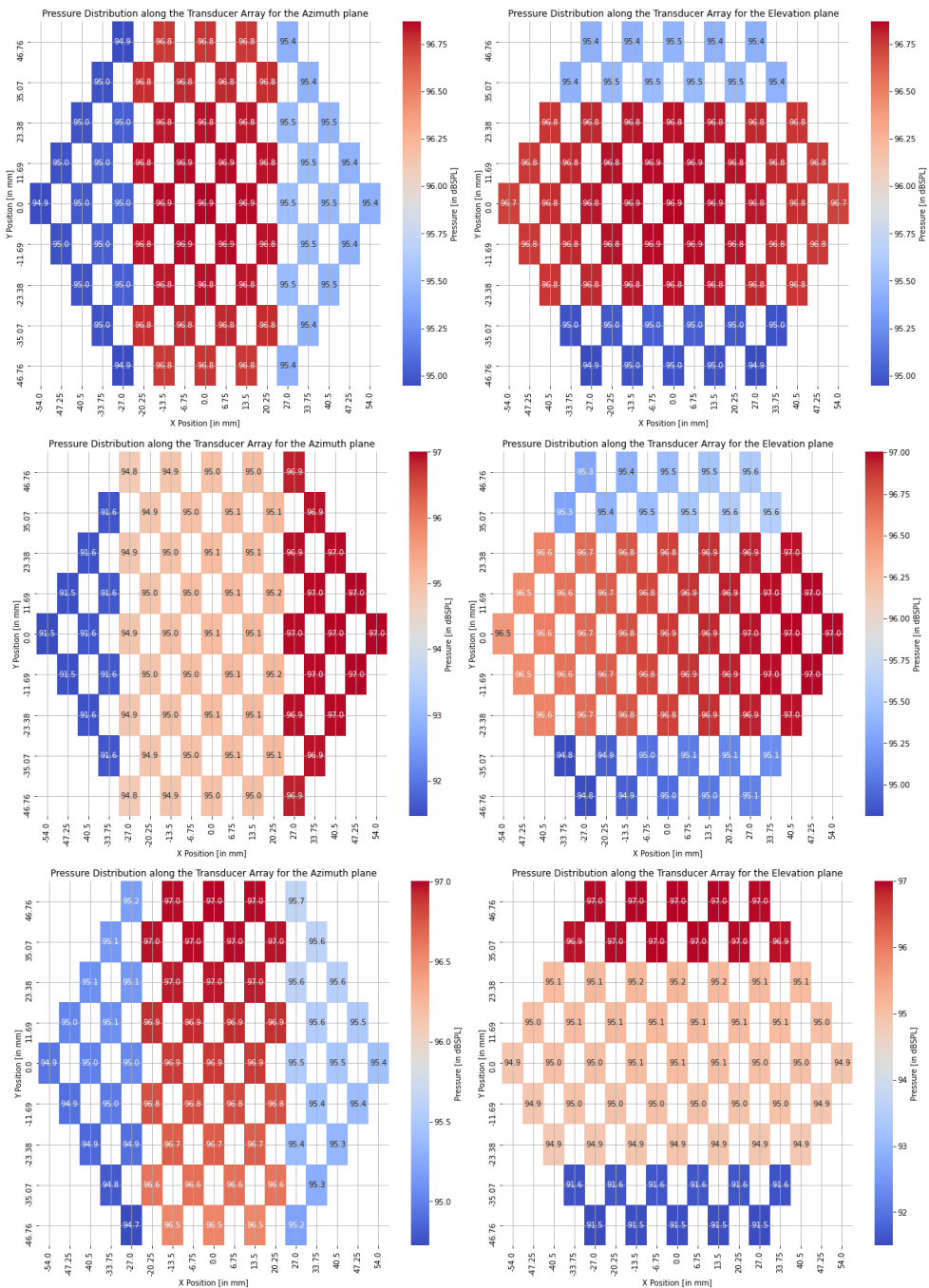


Figure 15: Pressure distribution along the hexagonal array for the azimuth (left) and elevation (right) planes for LP(0|0|30cm) (uppermost row) and at a 10° difference with respect to the other one on each plane (azimuth on the middle row; and elevation on the lowermost one) considering a 40kHz signal.

Furthermore, it is also possible to note that the directivity keeps increasing when incrementing the distance from the source to the LP. This is due to the inverse proportionality between the pressure and the separation between the array and the LP of the linear model. So, the overall level will be greater when closer to the source; ergo, a decrease will occur when doing the opposite. Thus, when reducing the distance from the array to the LP, the directivity is also reduced, leading to an increase of the width of the main lobe (Fig. 17 right).

So, considering this previous statement, it makes sense to incorporate a curvature to the array to

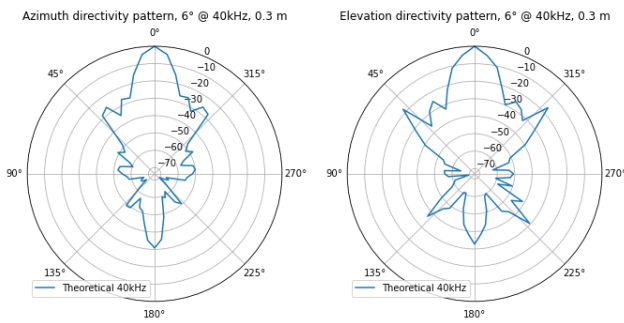


Figure 16: Theoretical directivity patterns for the azimuth (left) and elevation (right) planes for a 40kHz signal.

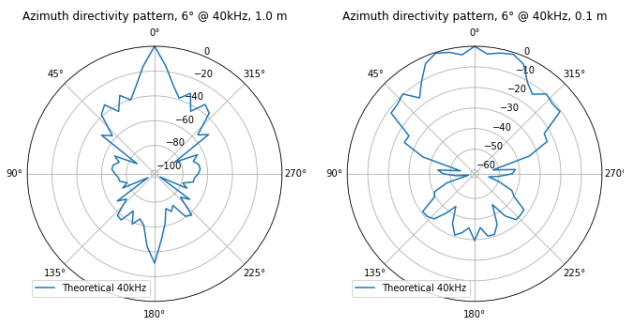


Figure 17: Simulated directivity pattern of a 40kHz signal propagating from the hexagonal array to a 1m (left) and a 10cm (right) LP.

modify the distance ratios from each transducer to the LP, thus, providing some control on the directivity and the pressure level provided by the array. This is corroborated by the data presented in Tab. 2, which shows the corresponding pressure levels for the curved array. Here, it is clear to note that the pre-existing inverse proportionality between distance and pressure is altered; the maximum is now located at the focus of the curvature of the array at the 30cm mark instead of at the closest point to the source.

Listening Point	Pressure Level
LP(0 0 10cm)	120 dB SPL
LP(0 0 30cm)	132 dB SPL
LP(0 0 1m)	115.6 dB SPL

Table 2: Pressure levels at different distances from the origin in the curved array configuration for a 40kHz signal.

Moreover, the directivity patterns at the different distances are also modified, as illustrated in Fig. 18. Although the directivity at distances different than the focal point of the parabolic behaviour of the array configuration are reduced; the main lobe for the 30cm pattern becomes narrower. This is result of the pressure level disparity created by the additional distance of some of the transducers to the LP.

6.4 Experimental results for the hexagonal array

On the other hand, several experiments are carried out to compare the theoretical model to the real behaviour of the parametric loudspeaker.

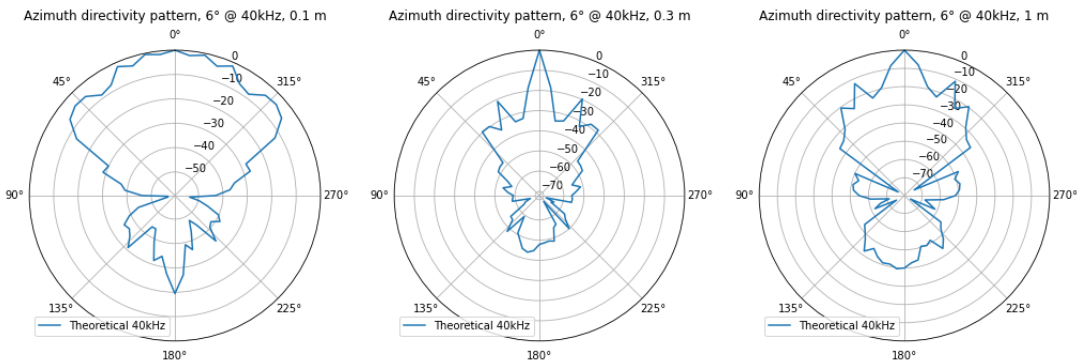


Figure 18: Directivity patterns for a 40kHz signal measured at 10cm , 30cm and 1m (from left to right, respectively) for the curved array.

6.4.1 Carrier signal frequency selection

First, to complete the following experiments, it is necessary to determine the impact of the carrier signal frequency for encoding the audible signal to maximize the efficiency of the loudspeaker. Literature suggests the utilization of the ultrasonic transducers' resonance frequency as that of the carrier signal [11] [14]. So, to verify the veracity and impact of this factor, some FRF measurements are taken for carrier signals that are slightly below (35kHz) and above (45kHz) the resonance (40.29kHz); the results are shown in Fig. 19.

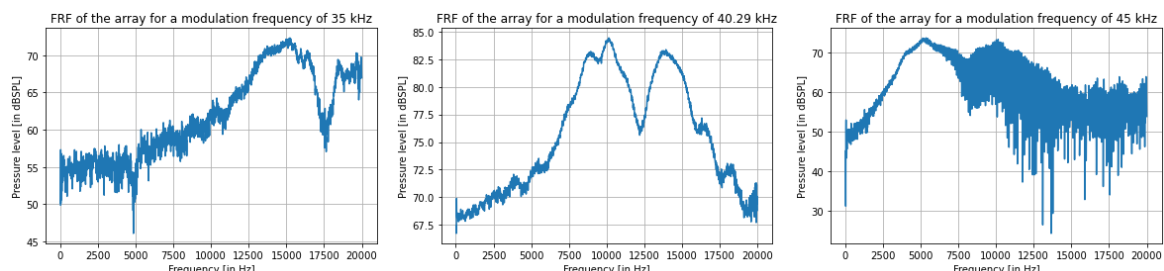


Figure 19: FRF of the array for different modulation frequencies: 35kHz , resonance and 45kHz (from left to right, correspondingly).

As expected, the results farther from the resonance frequency show a significant shift of the main features (the dip present at 12.5kHz , as well as the crests near it for the plot in the middle) of the FRF by around 5kHz . Also, there is a relevant decrease in the overall amplitude, which matches the behaviour presented by the transducers themselves in Fig. 6. However, this reduction is more meaningful along the frequency midrange, reducing the pressure level to magnitudes similar to the noise-like behaviour present at low and high frequencies of the FRF. This leads to the more distorted FRFs for the other carrier signal frequencies.

6.4.2 Pressure level with respect to distance

Furthermore, the axial sound pressure curves for some frequencies is determined, i.e. the pressure level is measured at different distances from the source. The result is depicted in Fig. 20, where one can notice a great reduction in amplitude for the 20kHz frequency behaviour. This is, probably, due to the interaction of the modulation and demodulation IMD components near that particular frequency, as it corresponds to half of that of the carrier signal.

Moreover, it is possible to observe that lower frequencies tend to have a greater amplitude at shorter distances. Such comportment is the result of the demodulation of the signal by the non-linearities of the transducers themselves (meaning its stiffness, electrical impedance, the membrane composition, etc.). Albeit linear theory suggest an invertly proportional behaviour between the propagation distance and pressure level, there is an unexpected behaviour for the 20Hz curve that suggest further investigation and knowledge of non-linear behaviour. Nevertheless, it is relevant to note that the data gathered for distances greater than 2m was mensurated under different conditions than the rest, because of the geometrical restrictions of the anechoic room. So, with the purpose of having a sense for the spatial restrictions of the loudspeaker, the remaining measurements were conducted in a non-controlled environment. This may be the reason for some the aforementioned behaviour, as well as that for the 15m peaks.

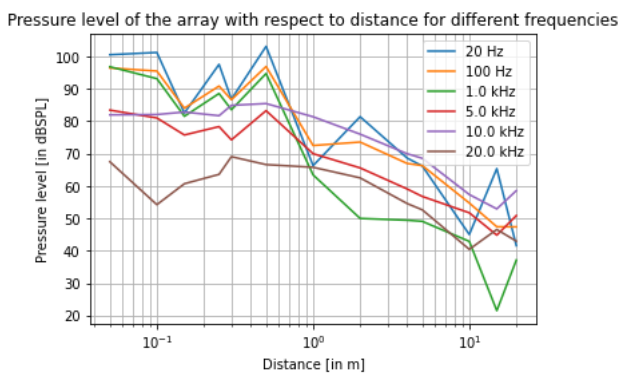


Figure 20: Pressure level with respect to distance for 100Hz , 1kHz , 5kHz and 10kHz

Still, one can notice that the overall shape is the decaying behaviour of the pressure due to its propagation. However, the air demodulation component is also palpable starting at around 50cm , as an increase in level can be observed as frequency increases. Moreover, the dip at 15cm may be due to interference patterns of the linear model or even due to non-linearities not considered in the model.

Although the shape is very similar to what is suggested in non-linear theory, especially for mid-to-high frequencies, the impact of the air demodulation is present at a much lower distance when comparing to what is presented in works like [6]. This might be because of the array size or even caused by different air non-linearities due to temperature, humidity, etc., as they have a significant impact on the air absorption and, ergo, the sound propagation as well [14] .

6.4.3 Directivity patterns

With this information, one can choose a distance at which the demodulation effect is present and compare the result to one for which it is not. Due to the design of the curved array, 30cm is elected for the latter case, whereas 1m is chosen for its counterpart, as the size of the anechoic room at the disposal allows it. For this, the same frequencies as for Fig. 20, except for 20Hz and 20kHz are chosen to facilitate the analysis of the data. The justification for the exclusion is that these frequencies present unquantifiable non-linearities distorting the responses. So, the directivity patterns are shown in Fig. 21.

So, when analyzing these graphs, one can observe how the pressure level difference at both distances wanes as the frequency increases. The reason for this is that, at low frequencies, the transducers' non-linearities demodulate the sound, which dissipates for larger distances. Thus, as the frequency increases, this effect is not noticeable and the directivity pattern becomes more independent on the distance to the source. The explicit values are presented in Tab. 3, where the increase in pressure level is clear at 1m . This is due to the fact that high frequencies are less prompt for dissipation at large distances, which

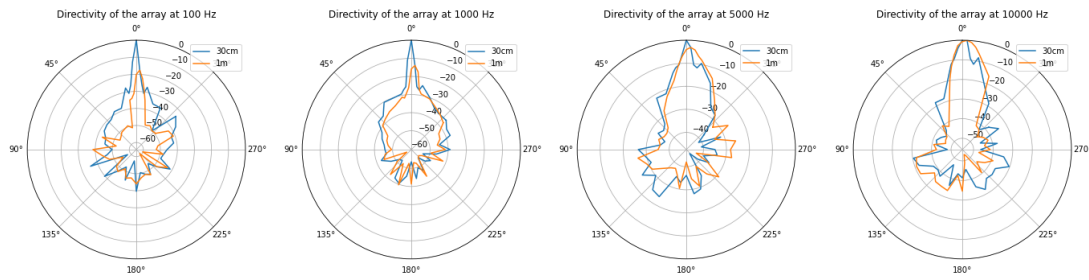


Figure 21: Directivity patterns at 30cm (blue) and 1m (orange) for 100Hz, 1kHz, 5kHz and 10kHz (from left to right, respectively).

is also validated by the linear model. However, at 30cm, the effect of the near-field non-linearities leads to a different behaviour.

Frequency	30 cm	1 m
100 Hz	86.8 dB SPL	69.3 dB SPL
1 kHz	84.1 dB SPL	70.2 dB SPL
5 kHz	75.0 dB SPL	71.9 dB SPL
10 kHz	85.1 dB SPL	85.1 dB SPL

Table 3: Experimental pressure levels at different distances and frequencies for the hexagonal array.

Furthermore, an unexpected fact is that the directivity decreases as frequency increases, as contrary to linear theory. This is the result of further effects of the transducers' non-linearities that are more pronounced at higher frequencies. "Any additional output from the transducer that is directly audible will behave like a traditional piston source, weakening the hyperdirectivity caused by parametric generation" [13]. So, even though the simulated directivity patterns presented in Figs. 16 and 17 provide a sense of the directivity of the acoustic beams, the linear model is not enough to properly predict the propagation of the sound waves for the different audible frequencies. Especially, as the non-linearities provide a much higher directivity at lower frequencies instead of the omnidirectional one suggested by the linear one.

6.5 Experimental results for the curved array

On the other hand, in order to check the impact of the curvature in the transducer array, the experiments carried out for the hexagonal configuration are repeated for the alternative, curved model (in Fig. 12 (right)).

6.5.1 Pressure level with respect to distance

Similarly and under the same conditions as the other array configuration, the pressure level is measured for the curved alternative. However, it is completed for distances restricted to those from the anechoic room to increase the veracity of the results and not be mistaken by effects of an echoic environment. The results are depicted in Fig. 22.

Here, it is possible to note an overall increase in pressure level for all frequencies for distances less or equal to 30cm with respect to the hexagonal array; although, this effect is greater for higher frequencies. Moreover, the opposite occurs for the 1m measurements, which matches the simulation results.

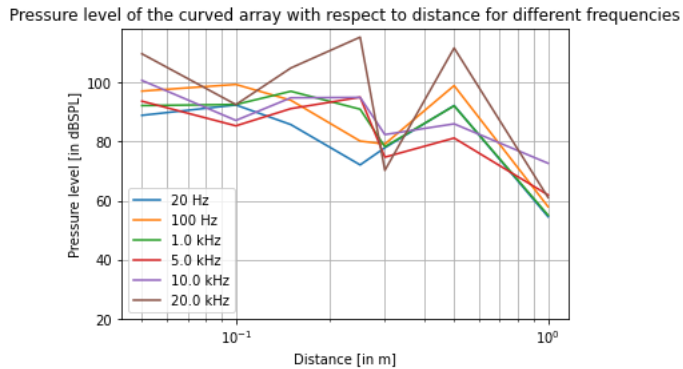


Figure 22: Pressure level at different distances and frequencies for the curved array configuration.

Nonetheless, a behaviour that is not predicted by the linear (or even the regular non-linear) model is that of the 20kHz signal, as it shows very strong peaks. This may be the result of the IMD interaction, whose effects are more prominent due to the distance alterations from the transducers to the LP.

6.5.2 Directivity patterns

On the same note, the directivity experiments are completed with the same characteristics and restrictions as before. The results corresponding to the same frequencies as those presented for the hexagonal array are illustrated in Fig. 23. One aspect to highlight is that the measurements for angles between $(90^\circ; 270^\circ)$ are neglected in this case, because of scheduling restrictions of the anechoic room; also, that particular range mostly encompasses noise and unwanted reflections, which are unnecessary for the analysis anyways.

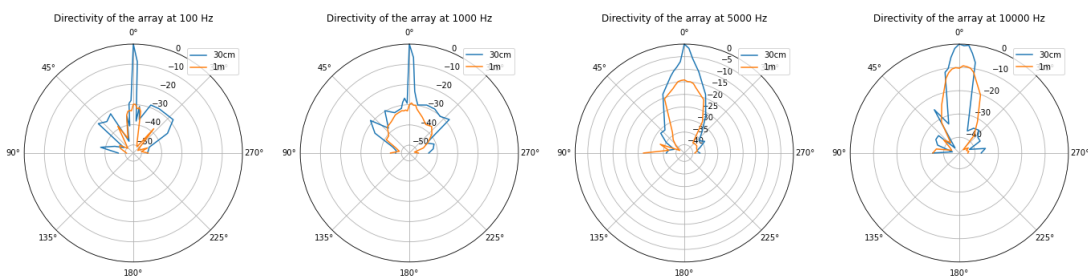


Figure 23: Directivity patterns at 30cm (blue) and 1m (orange) for 100Hz , 1kHz , 5kHz and 10kHz (from left to right respectively) for the curved array.

So, as expected by literature and the simulation, the shape of the array does have a relevant impact on the the directivity of the loudspeaker; the pressure level discrepancy between both measurement points is greater than that of the hexagonal array. Plus, the width of the main lobe at 30cm is greatly reduced for all frequencies with respect to its hexagonal counterpart.

However, the way it impacts the data differs greatly between the simulation using the linear model and the experimental data. The main difference lays in the fact that the curvature does not lead to an increase in pressure level at the focal point of the parabola like in Fig. 18; in fact, at some frequencies it is even attenuated (see Tab. 4). Also, the decrease in amplitude is more prominent for distances greater than the focal point of the array (like for the 1m measurements).

Nevertheless, this matches statements from non-linear theory [20] [17]. Additionally, it also dictates that the global noise level can be reduced by choosing the focus to create an exact anti-noise

source configured at the noise point. Nevertheless, this type of analysis is outside the scope of this project.

Frequency	30 cm	1 m
100 Hz	87.8 dB SPL	58.0 dB SPL
1 kHz	84.9 dB SPL	55.8 dB SPL
5 kHz	76.5 dB SPL	62.2 dB SPL
10 kHz	83.0 dB SPL	73.8 dB SPL

Table 4: Experimental pressure levels at different distances and frequencies for the curved array.

7 Additional system components

In order to construct an integral prototype, some additional components need to be added to increase its functionality. To begin with, the sound chain of the system presented in Fig. 24 will be explained along the function of each component and some other subsystems added in the project.

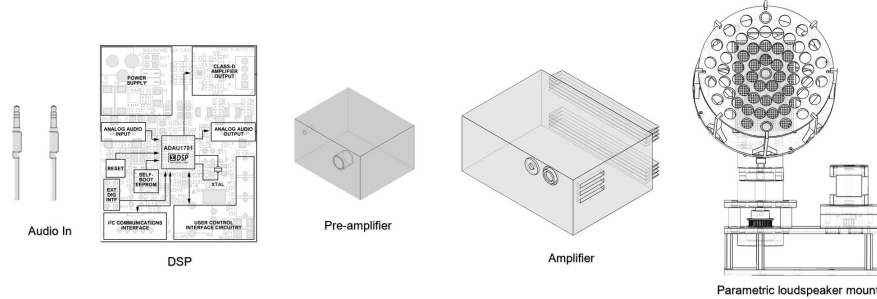


Figure 24: Sound chain for the parametric loudspeaker system.

7.1 Audio input

To begin with, the system has a conventional 3.5mm auxiliary input. The main reason to use this is to provide a standard audio input in order to be compatible with most handheld devices such as tablets and cellphones. The output amplitude of this signal uses voltages between 0 and $1V_{rms}$ as input signal for the Digital Signal Processor (DSP).

7.2 DSP

Once the message signal enters the system, it is time for the ADAU1701 digital audio processor to control and deliver a useful output signal to the pre-amp. The main advantage of using a DSP in the system is the ability to program it to deliver a modulated signal, in this case, using DSB-AM.

In addition to that, a gain control block is added in order to provide the user a better control over the system parameters by using I2C communication between the processor and microcontroller, as it will be explained in further subsections. An example is the ability to control the output volume in a digital way rather than in analog one.

However, an important note to consider is the amplitude level of the processor as it shows a maximum output voltage value of $300mV_{rms}$. This signal is too low for the loudspeaker, as the audible

level results insufficient, thus an increase of the signal level must be done before delivering it to the parametric array via a pre-amp.

7.3 Pre-amplifier

The main need for this stage is to increase the modulated signal even further, as the fixed gain of the amplifier does not yield decent audible results. So, the pre-amplifier, a simple non-inverting Op-Amp configuration (as the one illustrated in Fig. 25) is elected due to its simplicity, efficiency and PCB size.

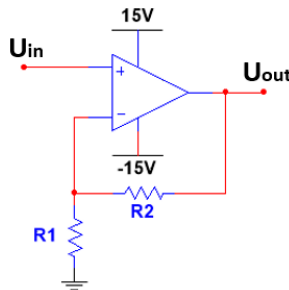


Figure 25: Non-inverting Op-Amp configuration used for the pre-amplifier.

So, considering the power amplifier's saturation point, the DSP's output voltage and the resistor selection, Eq. 5 is used to obtain a gain of 11. Leading to the following values: $R_1 = 1k\Omega$ and $R_2 = 10k\Omega$. Thus, the output of the pre-amp stage is then $3.3V_{rms}$.

$$G = 1 + \frac{R_2}{R_1} = 11 \quad (5)$$

Moreover, for simplicity, a 3.5mm female jack and a standard female coaxial connector is installed to facilitate the system integration. In addition to that, a Traco Power TMP 30215 AC/DC power module is integrated to this circuit to power the Op-Amp and to simplify the energy supply aspect of the module.

Furthermore, the characterization is elaborated based on the circuit illustrated in Fig. 26, where G_a and R_a indicate the amplifier's gain and resistance, respectively; U_e and U_{RL} the input and output voltages, correspondingly; and $R_L = 5.1\Omega$ is the resistance of a load. So, by plotting the input-output voltage ratio and by means of the expression for the voltage divider, one can obtain the behaviours for G_a and R_a with respect to frequency. They are presented in Fig. 27.

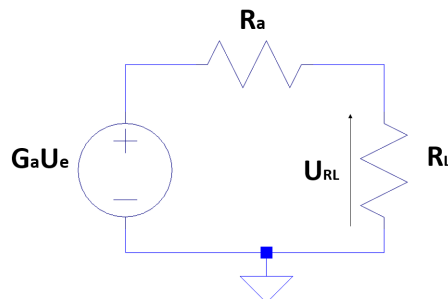


Figure 26: Circuit used to measure the amplifier's characteristics.

As can be observed, the gain decreases with frequency while the resistance increases. Since the DSP does not tolerate floating point values, the carrier signal frequency is set to $40kHz$. So, the gain and resistance will have values of around 10.99 and 72Ω , respectively.

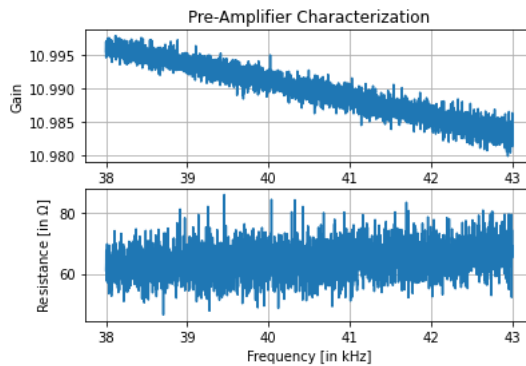


Figure 27: Gain (up) and internal resistance (down) of the pre-amplifier.

In addition to that, the saturation levels need to be determined to be able to maximize the amplification without deforming the signal produced. In this case, a $894mVrms$, $40kHz$ input signal results in saturation on the lower peak of the output signal (with $9.98Vrms$).

7.4 Power amplifier

In order to provide the elevated power level required for the parametric loudspeaker to produce audible sound, a power amplifier is needed. For this, a generic alternative provided by the university is chosen (as illustrated in Fig. 24); so, a datasheet is not available to verify the veracity of the obtained model.

Nevertheless, the characterization is elaborated in a similar manner as for the pre-amplifier. The results are presented in Fig. 28.

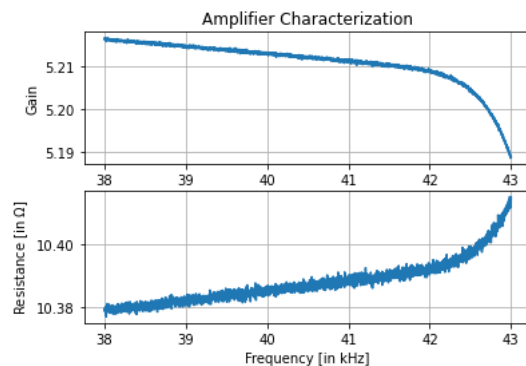


Figure 28: Gain (up) and internal resistance (down) of the power amplifier.

Here, one can notice a similar pattern in which the gain decreases and resistance increases as frequency increments. More specifically, at $40kHz$, a gain of 5.21 and a resistance of 10.385Ω is present. In this case, having a lower resistance benefits the system as a lower voltage is passing through it and allows most of the voltage to be used for the array.

Again, in a similar way to the previous stage, the saturation levels are also tested to avoid further distortion. This leads to a limit value for a $40kHz$ input signal of $3.6Vrms$, as this value starts to distort the lowermost peak of the output signal (with $17.9Vrms$).

7.5 Motors and WIFI Control

In order to direct the loudspeaker in two different planes (azimuth and elevation), two different motors are added to the system (see Fig. 29). The first one, a stepper motor driven at a 1/32 step resolution to be able to precisely control the azimuth direction, while a servomotor capable of a 180° rotation holds the transducer array providing elevation control.

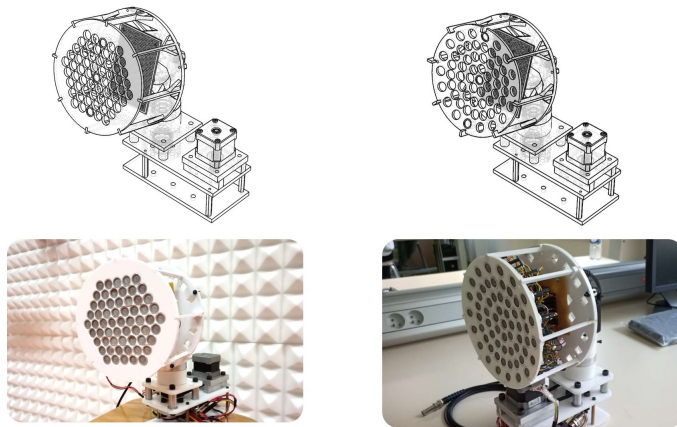


Figure 29: Hexagonal array configuration (left) and curved array configuration (right) final Prototypes

In order to provide the user a simple interface, the use of WIFI control is added in order to control the prototype motors and audio gain. In order to do this, the microprocessor *ESP8266* allows to configure it as an access point by sending HTML commands from a physical device (station) directly to the microprocessor. Also, one of its advantages is the compatibility with I2C that enables the volume control of the output signal, which can be achieved by means of a mobile device. For a general diagram on subsystems connection please refer to Fig. 30

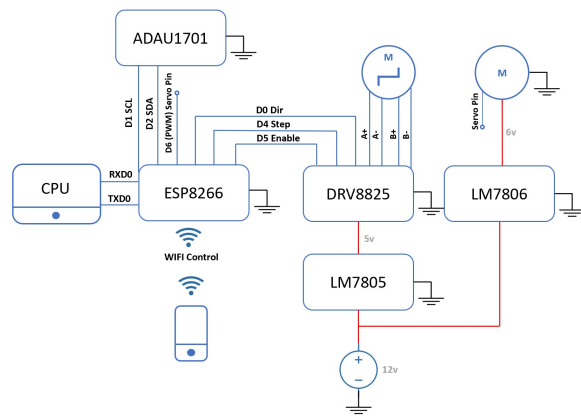


Figure 30: Subsystem Diagram for WIFI and Motor Control

8 Conclusions

By exploiting the non-linearities present in the air and the transducers themselves, it is possible to create a hyperdirective acoustic beam by modulating the message signal into an ultrasonic carrier one. It is important to highlight that, even though the linear model provides insight about the propagation of the audible signal, it still does not account for the non-linear effects that improve the system's response.

Nevertheless, even considering the effects of the air demodulation, there are still other aspects that factor into the actual response like the transducers' intrinsic non-linear comportment that decreases the width of the directivity pattern's main lobe, especially at low frequencies.

Furthermore, the overall shape of the transducer array has proven to be a simple way to have some further control for the directivity and sound pressure level, because this will lead to a different spatial pressure distribution and a lower noise level if choosing the parameters correctly.

Moreover, even though the exact mechanical model of the transducer was unknown, the SDOF model allows to have a decent representation of how one can explain the behaviour of the physical elements inside the transducer; similarly for the electrical one as well. From the acoustical point of view, it is important to use the transducers' resonance frequency (40.29kHz) as carrier signal to maximize the pressure level and particle velocity.

In this case, optimal efficiency of the AM in the loudspeaker may be achieved, reducing the power consumption of the system, the most relevant disadvantage of such a technology. However, another disadvantage of using parametric arrays is the low sound quality. Nevertheless, this can be easily ameliorated by decreasing the modulation index of the AM techniques, but also incrementing the power needed. These effects can also wane by using a more efficient modulation method.

On the other hand, it is important to remark that the using a DSP provides great versatility and improves the user experience altogether. Also, it dons the ability to make use of other modulation techniques which can be explored and tested for future work; it is also true for equalization and other signal treatment procedures as well.

The technology presented during this project has a great potential in the audio industry. As research and improvements on the subject progress, parametric loudspeakers could become a daily life product to reduce sound pollution and allow users to have either music or calls in a more private zone. With some improvements, it has the potential to become the next generation of loudspeakers.

9 Future work

The use of SSB-AM and a more thorough evaluation of the SRAM modulation methods should yield interesting, as they may produce a reduction of the impact of some problems like the distortion and/or power consumption. Furthermore, tests with an array with a curvature greater or equal to the experimental air demodulation distance, 50cm , should provide interesting results, as the impact of the nonlinearities of the transducer itself would not be present.

Moreover, an artificial intelligence is desired to localize a person's head and direct the sound beam to it in an automated way instead of using the mobile application. This would increase the speed and accuracy of the beam alignment, maximizing the efficiency of the parametric array.

Also, a comparison between two types of parametric loudspeakers is planned. This juxtaposition will contrast the "classic" model, the one presented in this work, using numerous ultrasonic transducers, and that using a PVDF-film-based acoustic transducer such as in [10] and [1]. With this, one could observe the main advantages and disadvantages of both alternatives. Additionally, an investigation on the feasibility of noise-cancelling technology using parametric arrays is also a promising topic.

Finally, an experimental comparison done under the same circumstances with a commercial parametric loudspeaker, like Ultrasonic's Acouspade Directional Sound System (available at the university). This way, one could compare the Fragor61T with an industry-quality product to have a sense of the benchmark of the project and contextualize it with the market.

A Measurement conditions



Figure 31: Experiment set-up for the directivity measurements performed at Le Mans University's semi-anechoic room for the hexagonal (upper-left) and curved arrays (upper-right), as well as for a single transducer (lower center).

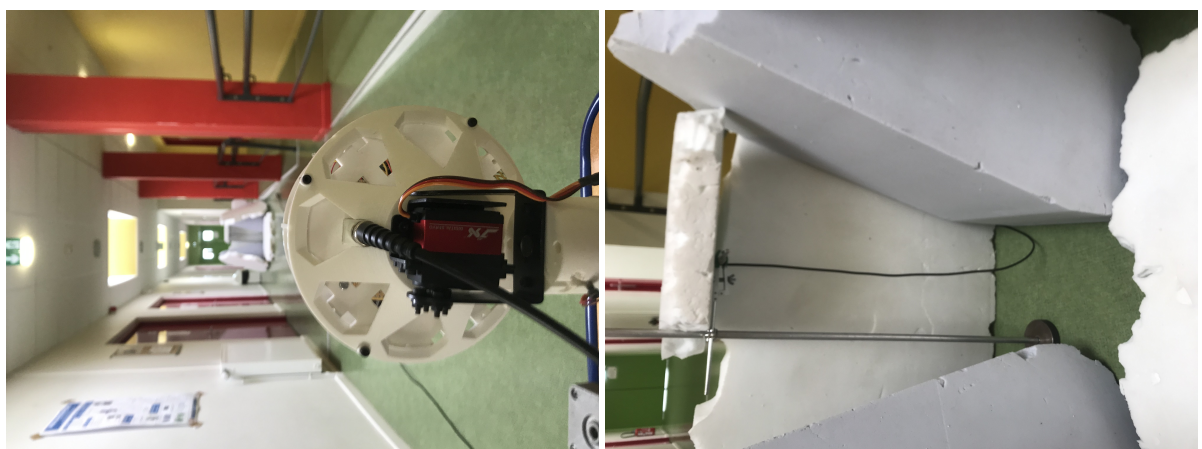


Figure 32: Measurement conditions of the pressure level at distances greater than 1m for the hexagonal array.

B Amplifier Gain

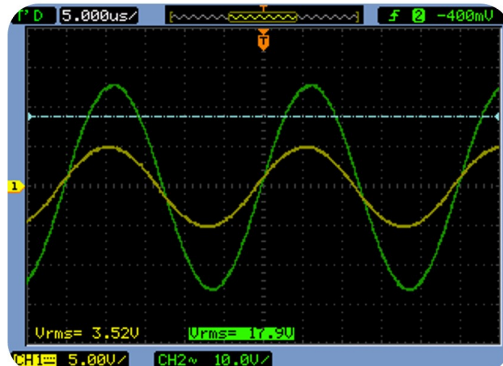


Figure 33: Amplifier voltage gain for a sine wave at 40kHz . Input (yellow) and output (green) voltages.

C Pressure distribution for the curved array

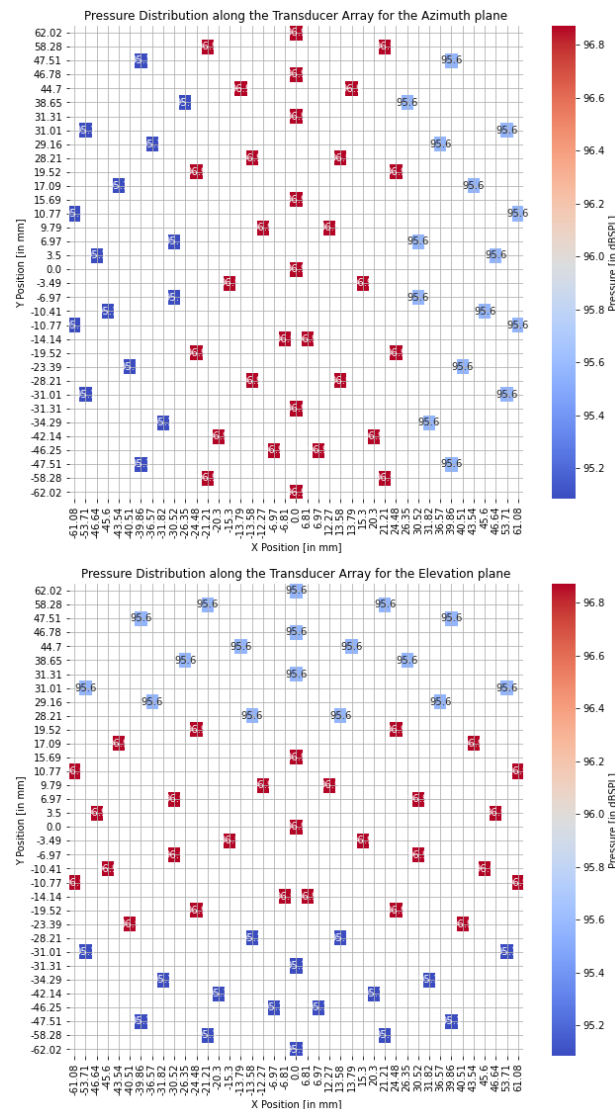


Figure 34: Pressure distribution along the curved array for the azimuth (up) and elevation (down) planes for LP(0|0|30cm) considering a 40kHz signal.

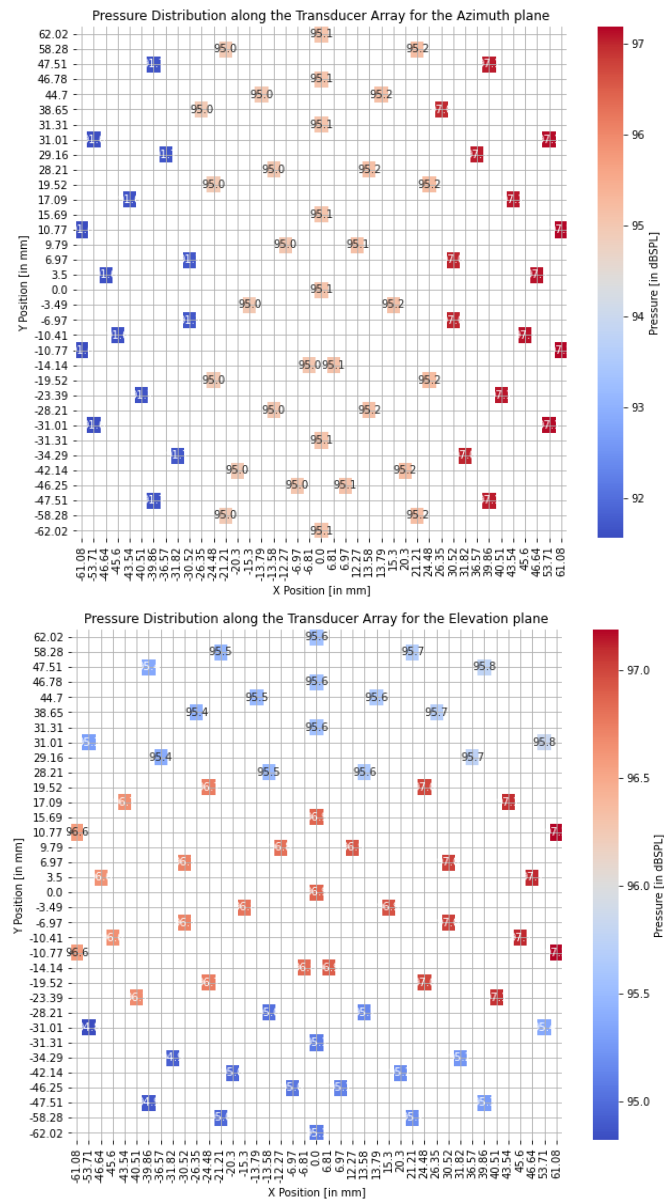


Figure 35: Pressure distribution along the curved array for the azimuth (up) and elevation (down) planes at a 10° difference with respect to LP(0|0|30cm) one on the azimuth plane for a 40kHz signal.

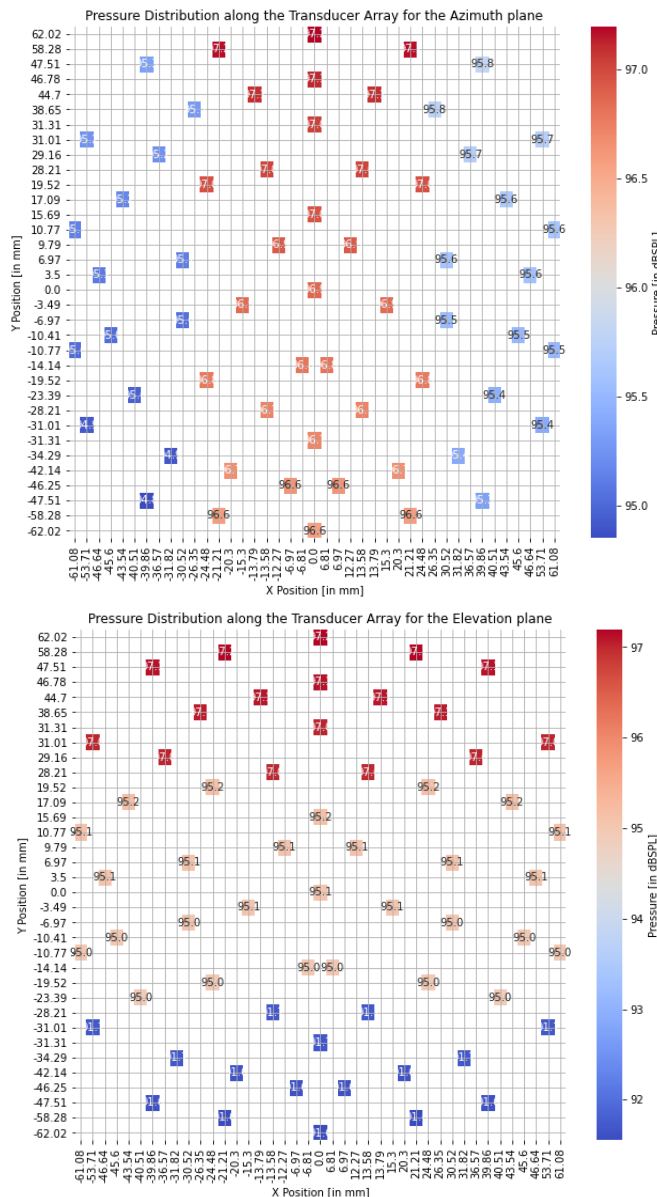


Figure 36: Pressure distribution along the curved array for the azimuth (up) and elevation (down) planes at a 10° difference with respect to LP(0|0|30cm) one on the elevation plane for a $40kHz$ signal.

References

- [1] P. Lotton A. Ritty, B. Gazengel and P. Hamery. Improvement of a directional loudspeaker by coupling of a piezoelectric film and acoustic cavities. In *19th International Congress on Acoustics*, 2007.
- [2] HO Berkay. Possible exploitation of non-linear acoustics in underwater transmitting applications. *Journal of Sound and Vibration*, 2(4):435–461, 1965.
- [3] Jose Cadavid and Antonin Novak. Practical problems in building parametric loudspeakers with ultrasonic piezoelectric emitters. In *Audio Engineering Society Convention 146*. Audio Engineering Society, 2019.

-
- [4] Bruce H Deatherage, Lloyd A Jeffress, and Hugh C Blodgett. A note on the audibility of intense ultrasonic sound. *The Journal of the Acoustical Society of America*, 26(4):582–582, 1954.
- [5] Felipe Farias and Waleed Abdulla. On rayleigh distance and absorption length of parametric loudspeakers. In *2015 Asia-Pacific Signal and Information Processing Association Annual Summit and Conference (APSIPA)*, pages 1262–1265. IEEE, 2015.
- [6] Woon-Seng Gan, Jun Yang, and Tomoo Kamakura. A review of parametric acoustic array in air. *Applied Acoustics*, 73(12):1211–1219, 2012.
- [7] Peifeng Ji, Ee-Leng Tan, Woon-Seng Gan, and Jun Yang. A comparative analysis of preprocessing methods for the parametric loudspeaker based on the khokhlov–zabolotskaya–kuznetsov equation for speech reproduction. *IEEE Transactions on audio, speech, and language processing*, 19(4):937–946, 2010.
- [8] Wei Ji, Woon-Seng Gan, and Peifeng Ji. Theoretical and experimental comparison of amplitude modulation techniques for parametric loudspeakers. In *Audio Engineering Society Convention 128*. Audio Engineering Society, 2010.
- [9] Thomas D Kite, John T Post, and Mark F Hamilton. Parametric array in air: Distortion reduction by preprocessing. *Proc. 16th int. cong. acoust*, 2:1091–1092, 1998.
- [10] Xu Limei, Cao Jianfang, and Huang Dagui. Design and characterization of a pvdf ultrasonic acoustic transducer applied in audio beam loudspeaker. In *IEEE International Conference Mechatronics and Automation, 2005*, volume 4, pages 1992–1997. IEEE, 2005.
- [11] Yusuke Nakashima, Takeshi Yoshimura, Nobuhiko Naka, and Tomoyuki Ohya. Prototype of mobile super directional loudspeaker. *NTT DoCoMo Tech J*, 8(1):25–32, 2006.
- [12] Dirk Olszewski and Klaus Linhard. 3g-3 optimum array configuration for parametric ultrasound loudspeakers using standard emitters. In *2006 IEEE Ultrasonics Symposium*, pages 657–660. IEEE, 2006.
- [13] F Joseph Pompei. The use of airborne ultrasonics for generating audible sound beams. *Journal of the Audio Engineering Society*, 47(9):726–731, 1999.
- [14] F Joseph Pompei. *Sound from ultrasound: The parametric array as an audible sound source*. PhD thesis, Massachusetts Institute of Technology, 2002.
- [15] Holosonics Research Labs. Audio Spotlight by Holosonics. Available at <https://www.holosonics.com/> (2021/05/10).
- [16] Ricardo San Martín, Pablo Tello, Ana Valencia, and Asier Marzo. Experimental evaluation of distortion in amplitude modulation techniques for parametric loudspeakers. *Applied Sciences*, 10(6):2070, 2020.
- [17] Chuang Shi, Yoshinobu Kajikawa, and Woon-Seng Gan. An overview of directivity control methods of the parametric array loudspeaker. *APSIPA Transactions on Signal and Information Processing*, 3, 2014.
- [18] Sascha Sporsa and Hagen Wierstorfb. A virtual endfire loudspeaker array for the generation of sound beams.
- [19] José Miguel CADAVID T. M2 IMDEA Project: Improvement of an Acoustical Parametric Array. 2018-2019.

- [20] Nobuo Tanaka and Motoki Tanaka. Mathematically trivial control of sound using a parametric beam focusing source. *The Journal of the Acoustical Society of America*, 129(1):165–172, 2011.
- [21] Peter J Westervelt. Parametric acoustic array. *The Journal of the Acoustical Society of America*, 35(4):535–537, 1963.
- [22] Masahide Yoneyama, Jun-ichiroh Fujimoto, Yu Kawamo, and Shoichi Sasabe. The audio spotlight: An application of nonlinear interaction of sound waves to a new type of loudspeaker design. *The Journal of the Acoustical Society of America*, 73(5):1532–1536, 1983.